PHYSICAL REVIEW A **83**, 051803(R) (2011)

Quantum ghost imaging through turbulence

P. Ben Dixon,[1] Gregory A. Howland,[1] Kam Wai Clifford Chan,[2] Colin O'Sullivan-Hale,[3] Brandon Rodenburg,[3] Nicholas D. Hardy,[4] Jeffrey H. Shapiro,[4] D. S. Simon,[5] A. V. Sergienko,[5] R. W. Boyd,[1,3] and John C. Howell[1]

[1]*Department of Physics and Astronomy, University of Rochester, Rochester, New York 14627, USA*

[2]*Rochester Optical Manufacturing Company, Rochester, New York 14606, USA*

[3]*Institute of Optics, University of Rochester, Rochester, New York 14627, USA*

[4]*Research Laboratory of Electronics, Massachusetts Institute of Technology, Cambridge, Massachusetts 02139, USA*

[5]*Department of Electrical & Computer Engineering, Boston University, Boston, Massachusetts 02215, USA*

(Received 3 February 2011; published 26 May 2011)

We investigate the effect of turbulence on quantum ghost imaging. We use entangled photons and demonstrate that for a specific experimental configuration the effect of turbulence can be greatly diminished. By decoupling the entangled photon source from the ghost-imaging central image plane, we are able to dramatically increase the ghost-image quality. When imaging a test pattern through turbulence, this method increases the imaged pattern visibility from $V = 0.15 \pm 0.04$ to 0.42 ± 0.04.

DOI: 10.1103/PhysRevA.83.051803 PACS number(s): 42.30.Va, 42.68.Bz, 03.67.Hk

I. INTRODUCTION

The phenomenon of ghost imaging (GI), observed by Pittman *et al.* in 1995 [1], is a method of generating the image of an object from correlation measurements. The experiment of Pittman *et al.* made use of pairs of entangled photons. One of the photons passed through a transmission object and then to a photon counter with no spatial resolution. The other photon passed directly to a spatially resolving photon counter. When looking at coincident photon detections, the detectors were able to see the object despite the fact that the object and the spatially resolving detector were in different arms of the experiment. While it was initially thought to be a quantum-mechanical effect reliant upon the entanglement between the two photons, similar results were later obtained using classical sources [2].

In addition to clarifying the boundary between quantum and classical effects [3–5], GI has been used for lensless imaging [6], superresolution [7,8], and entanglement detection [9]. More recently, research has recognized connections between GI and compressive sensing [10,11].

For many optical applications, imaging through turbulence is unavoidable [12,13]. GI is no different and research on the effect of turbulence on GI has recently witnessed a surge of interest [14–18]. In this paper we investigate experimentally the effect of turbulence on GI using entangled photons. We present an experimental demonstration that entangled-photon GI is affected by turbulence and how the effect can be reduced.

II. THEORY

The experimental apparatus is depicted in Fig. 1. A biphoton state $|\psi\rangle$ is created at a nonlinear crystal [19] and then split by a 50:50 beam splitter, sending the biphoton into two arms of the apparatus. In the object arm, the biphoton travels a distance $2f + \Delta$ to a lens that has focal length f. The biphoton then travels a distance $2f$ to a photon detector with no spatial resolution (a bucket detector). A transmission object, consisting of alternating opaque and clear vertical bars, is placed just in front of the detector. In the image arm, the biphoton travels a distance $2f - \Delta$ to a lens that again has focal length f. The biphoton then travels a distance $2f$ to a spatially resolving detector.

For $\Delta = 0$ the detectors and crystal are all located at image planes of each other. As one arm's lens-detector is moved toward the crystal by a distance Δ, the other arm's lens-detector is moved away by the same distance, keeping the sum of the arm's length constant (see Fig. 2).

Turbulent air flow is introduced into the beam path of the object arm. For turbulence between the crystal and the lens, it is a distance l_1 from the crystal (or a distance $l_1 - \Delta$ from the central image plane). For turbulence between the lens and the object, it is a distance $\Delta - l_1$ from the object.

The relevant function for GI is the second-order degree of coherence $G^{(2)}(x_1,x_2)$, where x_1 is a transverse position variable in the plane of the spatially resolving detector and x_2 is a transverse position variable in the plane of the bucket detector. We begin with the standard quantum-mechanical form and include an additional ensemble averaging—represented by outer angular brackets—to account for the statistical effect of turbulence:

$$G^{(2)}(x_1,x_2) = \langle\langle\psi|\hat{E}_i^\dagger(x_1)\hat{E}_s^\dagger(x_2)\hat{E}_s(x_2)\hat{E}_i(x_1)|\psi\rangle\rangle. \quad (1)$$

Neglecting overall normalization, this can be represented in the following way:

$$G^{(2)}(x_1,x_2) = \left\langle \int^{(4)} \psi^\star(\tilde{x}_s,\tilde{x}_i)H^\star(\tilde{x}_i,x_1)H^\star(\tilde{x}_s,x_2;\tilde{x}_t) \times H(x_s,x_2;x_t)H(x_i,x_1)\psi(x_s,x_i)d\tilde{x}_i d\tilde{x}_s dx_s dx_i \right\rangle. \quad (2)$$

Subscripts s and i indicate variables in the crystal plane and subscript t indicates variables in the plane of the turbulence. The function $\psi(x_s,x_i)$ is the transverse biphoton wave function, which we approximate as a plane wave with δ-function correlations $\psi(x_s,x_1) = \delta(x_s - x_i)$. The function $H(x_s,x_2;x_t)$ is a propagation operator going from the crystal plane to the object arm detection plane, passing through the plane of turbulence; $H(x_i,x_1)$ is a propagation operator going from the

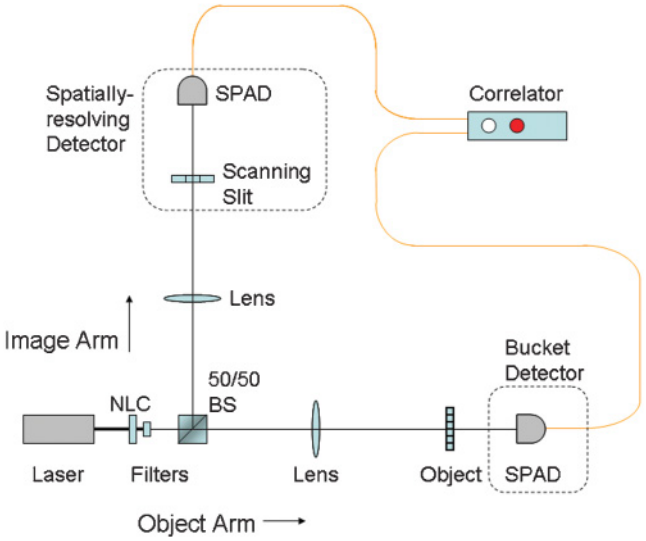

FIG. 1. (Color online) Experimental apparatus: A pump beam undergoes spontaneous parametric down-conversion (SPDC) at a nonlinear crystal (NLC) and the output passes a beam splitter (BS). One beam is sent through a lens and onto a transmission object. The other beam is sent through a lens and onto a scanning slit. The ghost image of the object is profiled by the slit. Photons are detected with single-photon avalanche diodes (SPADs). Detection events are then correlated.

crystal plane to the image arm detection plane. These operators can be represented in the following way:

$$H(x_s,x_2;x_t) = \int \exp\left(\frac{-ik(x_2-x_t)^2}{2(l_1-\Delta)}\right)\hat{T}(x_t) \times \exp\left(\frac{ik(x_t-x_s)^2}{2l_1}\right)dx_t, \quad (3)$$

$$H(x_i,x_1) = \exp\left(\frac{-ik}{2\Delta}(x_i-x_1)^2\right). \quad (4)$$

In our theoretical treatment, we assume a narrow sheet of turbulent air, whose effect on propagation can be characterized by a multiplicative operator $\hat{T}(x_t)$. We also assume that the lenses are sufficiently large that they capture all of the light from the spontaneous parametric down-conversion (SPDC) source. As a result, both turbulence locations in Fig. 2 are governed by the same operators.

We model the turbulence as a $\frac{6}{3}$ scaling law effect: $\langle\hat{T}^\star(\tilde{x}_t)\hat{T}(x_t)\rangle = \exp[-\alpha\,(x_t-\tilde{x}_t)^2/2]$, where α parametrizes the strength of the turbulence and has units $1/\mathrm{m}^2$ [12,13]. The resulting expression for $G^{(2)}(x_1,x_2)$ is

$$G^{(2)}(x_1,x_2) = \exp\left(\frac{-k^2(x_1-x_2)^2}{2\alpha(l_1-\Delta)^2}\right). \quad (5)$$

The ghost image $I(x_1)$ is then the product of the object and $G^{(2)}(x_1,x_2)$, integrated over x_2. We represent the object as $O(x_2) = \exp\left(-x_2^2/2w^2\right)\left[1+\cos(k_o x_2)\right]$. Here w is the spatial width of the illuminating beam and k_o is wave number

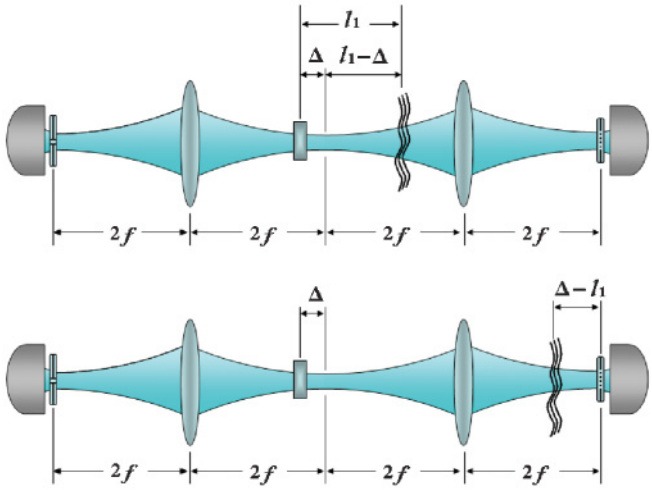

FIG. 2. (Color online) The experiment is shown conceptually using the Klyshko picture [20]; the object (on the right) is ghost imaged onto the scanning slit (on the left). The nonlinear crystal is offset from the central image plane by a distance Δ. The top picture shows the turbulence (represented by wavy lines) between the crystal and the lens. The bottom picture shows the turbulence located between the lens and the object. Experimentally relevant distances are labeled.

for the object's pattern spacing. Assuming $(l_1-\Delta)\sqrt{\alpha} \ll kw$, the ghost image is found to be

$$I(x_1) = \exp\left[-\frac{1}{2}\left(\frac{x_1}{w}\right)^2\right][1+V\cos(k_o\,x_1)]. \quad (6)$$

$I(x_1)$ has the same form as $O(x_1)$ with the object's unity visibility replaced by the GI visibility V:

$$V = g\exp\left(\frac{-\alpha\left(l_1-\Delta\right)^2}{2\left(k/k_o\right)^2}\right), \quad (7)$$

where g is the the optimum GI visibility with no turbulence. As either the turbulence increases in strength (increasing α) or the turbulence is moved away from the central image plane or the detector (increasing $l_1-\Delta$), the detected visibility V decreases, thus obscuring the detected pattern.

III. EXPERIMENT

Collimated light from a 3-mW, 325-nm HeCd laser with a $1/e^2$ full width of approximately 1600 μm pumped a 10-mm-thick β-BaB_2O_4 nonlinear crystal. The crystal was oriented for degenerate type-I collinear SPDC. After the crystal, the pump beam was blocked by colored glass filters and the SPDC bandwidth was limited by a 3-nm-wide spectral filter centered at 650 nm. The remaining SPDC beam was split into two arms by a 50:50 beam splitter.

In the image arm, a lens was located 1000 mm $-\,\Delta$ from the crystal; in the object arm, a lens was located 1000 mm $+\,\Delta$ from the crystal. Both lenses had focal length $f = 500$ mm. Detectors were located 1000 mm from the lenses.

The transmission object was a test pattern located 1000 mm from the lens. The bucket detector consisted of a 10× microscope objective that collected the transmitted light into a multimode optical fiber. The pattern had unit visibility

and 3.6 cycles/mm, which resulted in an object pattern wave number of $k_o = 7.2 \times \pi$ mm^{-1}. The spatially resolving detector consisted of a computer-controlled scanning slit located 1000 mm from the lens, which was again followed by a 10× microscope objective that collected light into a multimode optical fiber. The slit was approximately 40 μm wide and was scanned in 5-μm increments, giving spatial resolution.

The optical fibers were connected to Perkin Elmer single-photon detectors. The outputs of these detectors were time correlated using a PicoHarp 300 from PicoQuant. Photon counts were integrated at each slit location for 1–4 s. The spatially resolved coincident detections made up the ghost-image profiles.

A heat gun was mounted above the setup, providing turbulent air flow across the beam path. The effect of the turbulence was fitted to the model's wave structure function αx^2 [13]. From the fit we determined $\alpha = 2.5 \pm 1.5$ mm^{-2}. It should be noted that although our theoretical model makes use of a thin sheet of turbulence, experimentally the turbulent region was approximately 10 cm wide. The turbulence was therefore present for a significant portion of the apparatus arm.

Data were taken for an unshifted configuration with $\Delta = 0$ and for a shifted configuration with $\Delta = 330$ mm. In each configuration, ghost images were recorded with turbulence present in the object arm both between the crystal and lens and between the lens and the object. Ghost images were also recorded with no turbulence. The recorded ghost-image profiles were fitted to $I(x_1)$ from Eq. (6). The fit included a visibility term that constituted our measurement of the visibility V.

While allowing access to the central image plane of the apparatus, the shifted configuration introduced two experimental limitations: The detected flux decreased significantly as a result of the detectors being away from the beam focus and fewer spatial frequencies contributed to the ghost image as a result of the nonlinear crystal having a stronger aperturing effect.

Representative ghost images are shown in Fig. 3. With no turbulence, the unshifted configuration produced GI visibilities of 1.00 ± 0.05. The shifted configuration produced GI visibilities of only 0.65 ± 0.05. The scans also show the decreased flux and the broader beam profile associated with the shifted configuration.

Visibilities for turbulence between the lens and the object are shown in Fig. 4. When turbulence was close to the object, the observed visibility was near its no-turbulence levels. As the turbulence was moved away from the object, the GI visibility decreased. The visibility for the unshifted configuration remained above the visibility for the shifted configuration for all turbulence locations.

Visibilities for turbulence between the crystal and the lens are shown in Fig. 5. This is the main result of the experiment. Visibilities decreased as the turbulence was moved away from the crystal; however, the unshifted configuration had lower fringe visibility than the shifted configuration. Indeed, for turbulence located 432 mm from the crystal, the visibility was $V = 0.15 \pm 0.04$ for the unshifted configuration, while for the shifted configuration it was $V = 0.42 \pm 0.04$. Moving to the shifted configuration tripled the visibility. This effect

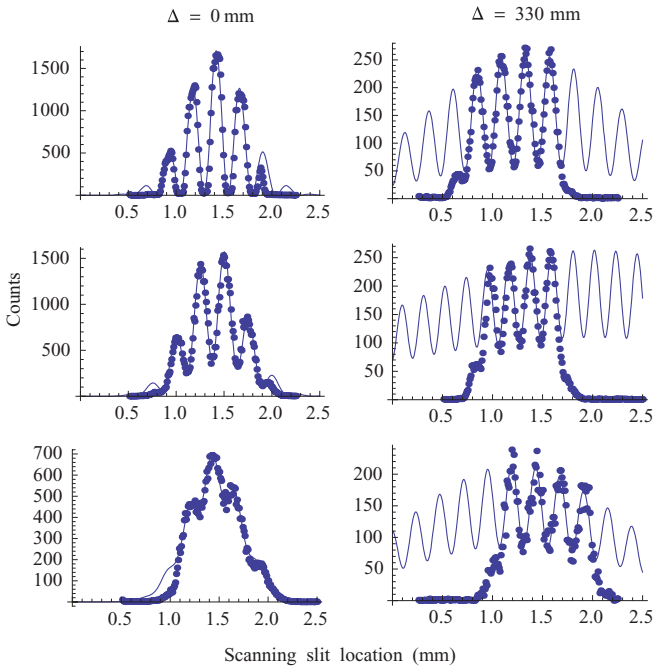

FIG. 3. (Color online) Representative ghost images for the unshifted configuration (left) and the shifted configuration (right). The top row shows images with no turbulence. The middle row shows images for turbulence between the lens and the object, 203 mm (right) and 229 mm (left) from the object. The bottom row shows images for turbulence between the crystal and the lens, 432 mm from the crystal. Points are experimental data while curves are fits to the data. Counts are measured in coincident photon detections per second.

can be understood physically by recognizing that the image of an object is unaffected by perturbing the phase of the illumination source—images consist of intensities only. By placing the turbulence near one of the image planes, it is as if

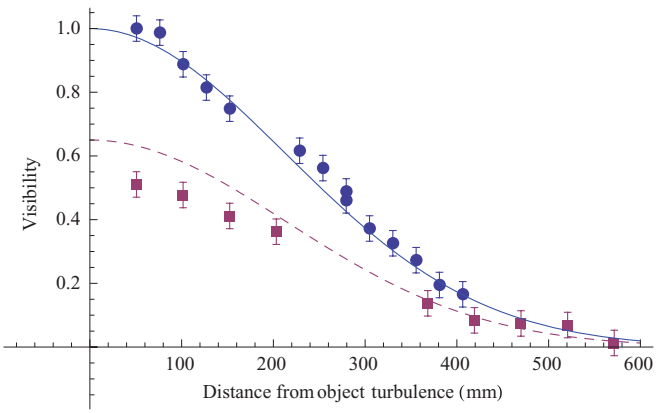

FIG. 4. (Color online) GI visibilities are shown for turbulence between the lens and the object. Visibilities are plotted as a function of distance from the object to the turbulence [$l_1 - \Delta$ in Eq. (7)]. Data for the unshifted configuration are shown as blue circles. Data for the shifted configuration are shown as purple squares. Curves are plots from Eq. (7). The solid curve is for the unshifted configuration, with $g = 1.00$. The dashed curve is for the shifted configuration, with $g = 0.65$. For both curves $\alpha = 2.0$ mm^{-2}.

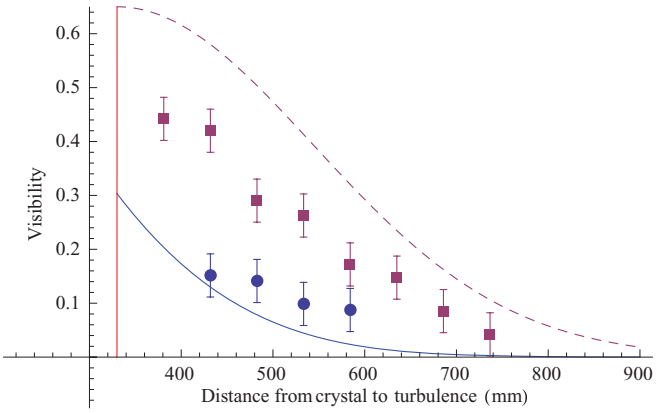

FIG. 5. (Color online) GI visibilities are shown for turbulence between the crystal and the lens. Visibilities are plotted as a function of distance from the crystal to the turbulence [l_1 in Eq. (7)]. Data for the unshifted configuration are shown as blue circles while data for the shifted configuration are shown as purple squares. Curves are plots from Eq. (7). The solid curve is for the unshifted configuration, with $g = 1.00$. The dashed curve is for the shifted configuration, with $g = 0.65$. For both curves $\alpha = 2.0\ \text{mm}^{-2}$. The vertical line marks the location of the central image plane.

we are perturbing the phase of the illumination source only, not the propagation.

IV. CONCLUSION

By moving the crystal from the central image plane we were able to place turbulence in this plane. This decreased the observed effect of turbulence; in fact, it more than made up for the inherent loss of visibility associated with the shifted configuration. This technique has use in free-space GI applications where turbulence is involved. By arranging detectors to place an image plane at the location of the turbulence, image degradation from the turbulence can be diminished. Although we used optical fields and turbulent airflow, our result applies to any type of propagating wave and a broad class of random or complex media including, for example, biological tissue or metamaterials.

Although we have used entangled photons, similar results are expected for thermal light GI. It should also be noted that the theoretical description assumes δ-function correlations for the biphoton state and a thin-region, non-Kolmogorov turbulence model [12,13,21]. We are currently extending our theoretical description to include different SPDC correlation areas and a more complex description of turbulence including the possibility of volume turbulence. The limitations of the theoretical description presented here do not extend to the experimental results; indeed, the biphoton state had a correlation size of approximately 50 μm. The turbulence was in reality volume turbulence approximately 10 cm in length and it did not truly have the Gaussian structure function of our approximation.

In this paper we have demonstrated a method of ameliorating the effects of turbulence on GI systems and have provided a theoretical model that accurately describes the experimental data. We shift the source of entangled photons away from a quantum GI system's central image plane and place turbulence near this plane. This dramatically increases the GI contrast. For turbulence located 432 mm from the crystal, this technique took the observed pattern visibility from $V = 0.15 \pm 0.04$ to 0.42 ± 0.04, thus tripling the system's imaging visibility.

ACKNOWLEDGMENTS

We acknowledge discussions with J.H. Eberly and support by DARPA DSO InPho Grant No. W911NF-10-1-0404 and USARO MURI Grant No. W911NF-05-1-0197.

[1] T. B. Pittman, Y. H. Shih, D. V. Strekalov, and A. V. Sergienko, Phys. Rev. A **52**, R3429 (1995).
[2] R. S. Bennink, S. J. Bentley, and R. W. Boyd, Phys. Rev. Lett. **89**, 113601 (2002).
[3] R. S. Bennink, S. J. Bentley, R. W. Boyd, and J. C. Howell, Phys. Rev. Lett. **92**, 033601 (2004).
[4] A. Gatti, E. Brambilla, M. Bache, and L. A. Lugiato, Phys. Rev. Lett. **93**, 093602 (2004).
[5] B. I. Erkmen and J. H. Shapiro, Phys. Rev. A **77**, 043809 (2008).
[6] G. Scarcelli, V. Berardi, and Y. Shih, Appl. Phys. Lett. **88**, 061106 (2006).
[7] F. Ferri, D. Magatti, A. Gatti, M. Bache, E. Brambilla, and L. A. Lugiato, Phys. Rev. Lett. **94**, 183602 (2005).
[8] I. Vidal, E. J. S. Fonseca, and J. M. Hickmann, Phys. Rev. A **82**, 043827 (2010).
[9] M. D'Angelo, Y. H. Kim, S. P. Kulik, and Y. Shih, Phys. Rev. Lett. **92**, 233601 (2004).
[10] J. H. Shapiro, Phys. Rev. A **78**, 061802(R) (2008).
[11] O. Katz, Y. Bromberg, and Y. Silberberg, Appl. Phys. Lett. **95**, 131110 (2009).
[12] V. I. Tatarski, *Wave Propagation in a Turbulent Medium* (McGraw-Hill, New York, 1961).
[13] R. L. Fante, Prog. Opt. **22**, 341 (1985).
[14] J. Cheng, Opt. Express **17**, 7916 (2009).
[15] C. Li, T. Wang, J. Pu, and R. Rao, Appl. Phys. B **99**, 599 (2010).
[16] P. Zhang, W. Gong, X. Shen, and S. Han, Phys. Rev. A **82**, 033817 (2010).
[17] R. E. Meyers, K. S. Deacon, and Y. Shih, Proc. SPIE **7815**, 781506 (2010).
[18] R. E. Meyers and K. S. Deacon, Proc. SPIE **7815**, 78150I (2010).
[19] D. N. Klyshko, Zh. Eksp. Teor. Fiz. **94**, 82 (1988) [Sov. Phys. JETP **67**, 1131 (1988)].
[20] D. N. Klyshko, Zh. Eksp. Teor. Fiz. **83**, 1313 (1982) [Sov. Phys. JETP **56**, 753 (1982)].
[21] A. N. Kolmogorov, C. R. Acad. Sci. URSS **30**, 301 (1941).